NUREG/CR-0169
EGG-2037

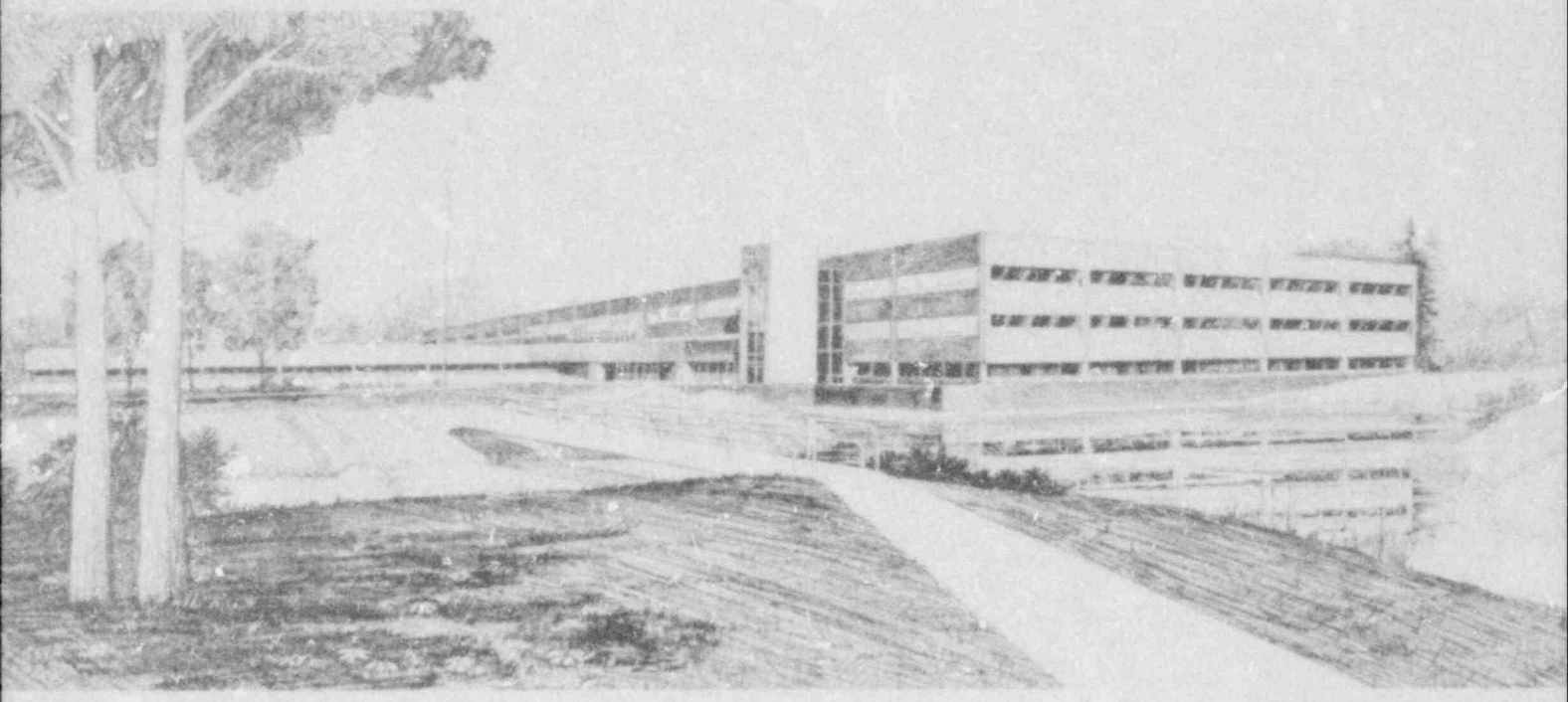

U.S. Department of Energy
Idaho Operations Office • Idaho National Engineering Laboratory

LOFT Experimental Measurements Uncertainty Analyses Volume XVIII Radiation-Hardened Gamma Densitometer

Gordon D. Lassahn

September 1980

Prepared for the
U.S. Nuclear Regulatory Commission
Under DOE Contract No. DE-AC07-76IDO1570

EG&G Idaho

Available from
U.S. Nuclear Regulatory Commission
Washington, D.C. 20555

Available from
National Technical Information Service
Springfield, Virginia 22161
Price: Printed Copy A10 Microfiche $3.00

The price of this document for requesters outside the North American continent can be obtained from the National Technical Information Service.

NUREG/CR-0169
EGG-2037
Distribution Category: R2

LOFT EXPERIMENTAL MEASUREMENTS UNCERTAINTY ANALYSES VOLUME XVIII RADIATION-HARDENED GAMMA DENSITOMETER

Gordon D. Lassahn

Published September 1980

EG&G Idaho, Inc.
Idaho Falls, Idaho 83415

Prepared for the
U.S. Nuclear Regulatory Commission
Washington, D. C. 20555
Under DOE Contract No. DE-AC07-76IDO1570
FIN No. A6043

ABSTRACT

The measurement uncertainty for the LOFT radiation-hardened gamma densitometer installed in the Loss-of-Fluid Test (LOFT) system is analyzed. These densitometers measure the fluid density in the LOFT primary coolant piping during the loss-of-coolant experiments. This measurement uncertainty analysis concluded that the random noise associated with the radiation process randomness and the bias uncertainty associated with the shim calibration procedure are the major sources of uncertainty in measurements made by the LOFT densitometers. The uncertainty ranges from 0.05 to 0.51 Mg/m^3, depending on experiment parameters.

FOREWORD

This document (NUREG/CR-0169, EGG-2037, Volume XVIII[a]) reports results of an uncertainty analysis for the radiation-hardened gamma densitometers installed in the Loss-of-Fluid Test (LOFT) system to measure fluid density in the primary coolant piping. Measurement uncertainty analyses are performed to evaluate the anticipated performance uncertainty for each experimental measurement in the LOFT system. Results of these analyses are reported in a series of volumes designated NUREG/CR-0169, EGG-2037. Volume I of this series will describe the LOFT experimental measurement systems and the technique used for calculating the uncertainties. The remaining volumes in the series will present detailed results from the uncertainty analysis performed for each experimental measurement system.

The following volumes have preceded Volume XVIII:

1. P. A. Quinn, G. L. Biladeau, R. Y. Maughan, *LOFT Experimental Measurements Uncertainty Analyses, Volume V, LOFT External Accelerometer Uncertainty Analysis*, NUREG/CR-0169, TREE-1089, October 1978.

2. G. L. Biladeau, *LOFT Experimental Measurements Uncertainty Analyses, Volume VI, LOFT Linear Variable Differential Transformer Displacement Transducer Uncertainty Analysis*, TREE-NUREG-1089, February 1978.

3. G. D. Lassahn, *LOFT Experimental Measurements Uncertainty Analyses, Volume VII, LOFT Self-Powered Neutron Detector Uncertainty Analysis*, NUREG/CR-0169, TREE-1089, August 1978.

4. G. D. Lassahn and P. A. Quinn, *LOFT Experimental Measurements Uncertainty Analyses, Volume VIII, LOFT Traversing In-Core Probe Uncertainty Analysis*, NUREG/CR-0169, TREE-1089, August 1978.

5. G. L. Biladeau, *LOFT Experimental Measurements Uncertainty Analyses, Volume IX, LOFT Strain Gage Uncertainty Analysis*, TREE-NUREG-1089, June 1978.

6. S. Silverman, *LOFT Experimental Measurements Uncertainty Analyses, Volume XIV, LOFT Drag Disc-Turbine Transducer Uncertainty Analysis*, NUREG/CR-0169, TREE-1089, November 1978.

7. L. D. Goodrich, *LOFT Experimental Measurements Uncertainty Analyses, Volume XV, LOFT Primary Coolant Pump Speed Measurement Uncertainty Analysis*, TREE-NUREG-1089, April 1978.

8. G. D. Lassahn, *LOFT Experimental Measurements Uncertainties Analyses, Volume XVI, LOFT Three-Beam Gamma Densitometer System*, TREE-NUREG-1089, February 1978.

---

a. Volumes VI, IX, XV, and XVI were published prior to implementation of the NUREG/CR numbering system as TREE-NUREG-1089. Volumes V, VII, VIII, and XIV were published as NUREG/CR-0169, TREE-1089 (TREE was the former designation for formal reports prepared by EG&G Idaho, Inc.). The remaining volumes in this series of uncertainty analyses will be published as NUREG/CR-0169, EGG-2037.

CONTENTS

FIGURES

TABLES

NOMENCLATURE

A	-	Coincidence-corrected A′
A′	-	Live-time-corrected photon count rate for the indicated energy range
a	-	Calibration coefficient
B	-	Without α or β subscript, total background radiation count rate
B	-	With α or β subscript, background radiation count rate in α or β energy range
b	-	Calibration coefficient
C	-	Without α or β subscript, total cobalt radiation count rate
C	-	With α or β subscript, cobalt radiation count rate in α or β energy range
F and G	-	Spectrum shape coefficients, used in coincidence correction
g	-	Label for gas phase or a substitute for the gas phase
I	-	Number of photons detected in one measurement period in the specified energy range, not live time corrected
i	-	Label for Beam i, i = 1, 2, 3, and 4 (corresponding to Beams A, B, C, and D)
K	-	Number of live time pulses generated by the live time clock during one measurement period
l	-	Label for the liquid phase
N and N′	-	Number of live time pulses counted by the system (N) and the amplifier (N′) live time counters during the measurement period
P	-	Total live-time-corrected photon count rate
P′	-	Total photon counts detected in the measurement period
R	-	A time characteristic of the electronics, nominally 125 ns
T	-	Length of the measurement period
X, Y, and Z	-	Symbols used to represent unspecified variables
α and β	-	Labels for the α and β energy ranges
μX	-	Average of X
ρ	-	Fluid density
σX	-	Standard deviation of X
τ and τ'	-	Live time fractions for the spectrum analyzer system (τ) and the amplifier alone (τ').

SUMMARY

The radiation-hardened gamma densitometers are designed to measure the density of the primary coolant at several different pi[illegible]locations on the Loss-of-Fluid Test (LOFT) system. The LOFT system includes a small-scale nuclear [illegible]ssurized water reactor and support systems designed to provide data from loss-of-coolant experiments.

The fluid density in the LOFT primary coolant piping is inferred from measurements of the intensities of beams of gamma radiation that pass through the fluid. The radiation source is approximately 11 curies of cobalt-60. Three gamma radiation detectors are arranged to detect beams of radiation that pass unscattered from the source, through the pipe and fluid, and into the detectors. A fourth detector is provided that cannot receive radiation directly from the cobalt source. All four detectors receive scattered cobalt radiation and various types of reactor background radiation. However, the radiation-hardened densitometers were designed to function in the presence of the radiation normally present around the nuclear reactor.

The dominant uncertainty component in the LOFT radiation-hardened densitometer is the randomness inherent in the radiation processes. This randomness causes a random noise uncertainty component in the calculated density values, of magnitude (2σ, or 95% confidence level) between 17 and 55 kg/m^3, depending on which beam is used and on the fluid density, for a 1-second data averaging time. In some experiments, there may also be a significant bias uncertainty associated with the calibration of the system.

LOFT EXPERIMENTAL MEASUREMENTS UNCERTAINTY ANALYSES VOLUME XVIII RADIATION-HARDENED GAMMA DENSITOMETER

1. INTRODUCTION

The radiation-hardened gamma densitometers discussed herein are designed to measure the density of the primary coolant at several different piping locations on the Loss-of-Fluid Test (LOFT) system. The fluid density is inferred from measurements of the intensities of beams of gamma radiation that pass through the fluid. The radiation-hardened densitometers were designed to function in the presence of the radiation normally present around the nuclear reactor.

The purpose of this report is to describe quantitatively the uncertainty, and its sources, in the fluid density measurements obtained from the LOFT radiation-hardened densitometers. The general procedure is to describe each recognized, potentially significant source of uncertainty and to analyze its effect on the final measurement result. (The measurement result, in the context of this report, is the density of the fluid averaged along each of the primary gamma radiation beam paths.) When there is some question about how large any uncertainty component is, the philosophy is to use the largest of the reasonable choices. Thus, the uncertainties quoted here should be regarded as upper bound estimates in questionable cases. As it turns out, the major uncertainty contributions are quite well understood, and these estimates are expected to be quite accurate.

The LOFT system[1] includes a small-scale nuclear pressurized water reactor and support systems designed to provide data from loss-of-coolant experiments. The LOFT system is located at the Idaho National Engineering Laboratory. The LOFT Experimental Program is conducted by EG&G Idaho, Inc., for the U.S. Nuclear Regulatory Commission and is administered by the U.S. Department of Energy. The instrumentation installed on the LOFT system provide data for evaluating the response of a pressurized water reactor system during loss-of-coolant transients. The radiation-hardened gamma densitometers currently installed on the LOFT system replace the simpler, nonradiation-hardened densitometers discussed in Reference 2. The positions of the three primary beams of gamma radiation are the only significant features common to the two types of densitometers.

The radiation-hardened gamma densitometers are described in Section 2. The procedures for analyzing the data from the densitometers are discussed in Section 3. The uncertainty estimates are presented in Section 4. The concluding statements and list of references are provided in Sections 5 and 6, respectively.

2. DENSITOMETER DESCRIPTION

The radiation-hardened gamma densitometer consists of a radiation source, detectors, shielding, and the electronics system used to process the detector signals. The arrangement of the source, detectors, and shielding when mounted on the LOFT piping is shown in Figure 1. The radiation source is approximately 11 curies of cobalt-60. Three gamma radiation detectors are arranged to detect radiation that passes unscattered from the source, through the pipe and fluid, and into the detectors. These three direct paths are called Beams A, B, and C. A fourth detector, referred to as Beam D, cannot receive radiation directly from the cobalt source. All four detectors receive scattered cobalt radiation and various types of reactor background radiation. Beams A, B, and C are in a plane perpendicular to the pipe axis. Beam D is tilted 11 degrees out of the perpendicular plane.

The cobalt radiation source can be moved, by remote control, into either the exposed position, which is the normal operating position, or the stored position, in which radiation cannot get from the source to the detectors. This feature allows certain useful calibrations and preliminary measurements, which are discussed in Section 3.

A thin tungsten plate, called a shim, can be inserted in front of the source to attenuate Beams A, B, and C by known amounts. This is sometimes used as a calibration aid.

Each radiation detector puts out an electrical pulse for each gamma photon interacting with the detector. (Sometimes pulses from several photons may overlap and appear as one pulse. This is referred to in this report as a pile-up event.) The densitometer electronics system that processes the pulses from the detectors is shown schematically in Figure 2. This system records four quantities for each densitometer beam for each measurement period as follows:

1. A pulse amplitude spectrum
2. A total pulse count P′
3. The amplifier live time count N′
4. The system live time count N.

A pulse amplitude spectrum is a record of the number of pulses accumulated in each of several contiguous pulse amplitude ranges. For Beams A, B, and C, the spectrum comprises 64 amplitude ranges or channels. A representative spectrum for Beam B is shown in Figure 3. A spectrum for Beam D comprises 512 channels. The total pulse count, P′, is the total number of pulses entering the amplifier during the measurement period.

The system live time count, N, is the number of clock pulses counted during the measurement period. These clock pulses are generated at the rate of 20 000 per second, but they are counted only when the system is live (ready to accept and process another pulse). Thus, the value of N is an indicator of the system's live time during the measurement period. The value of N′ indicates the live time of the amplifier in a similar manner.

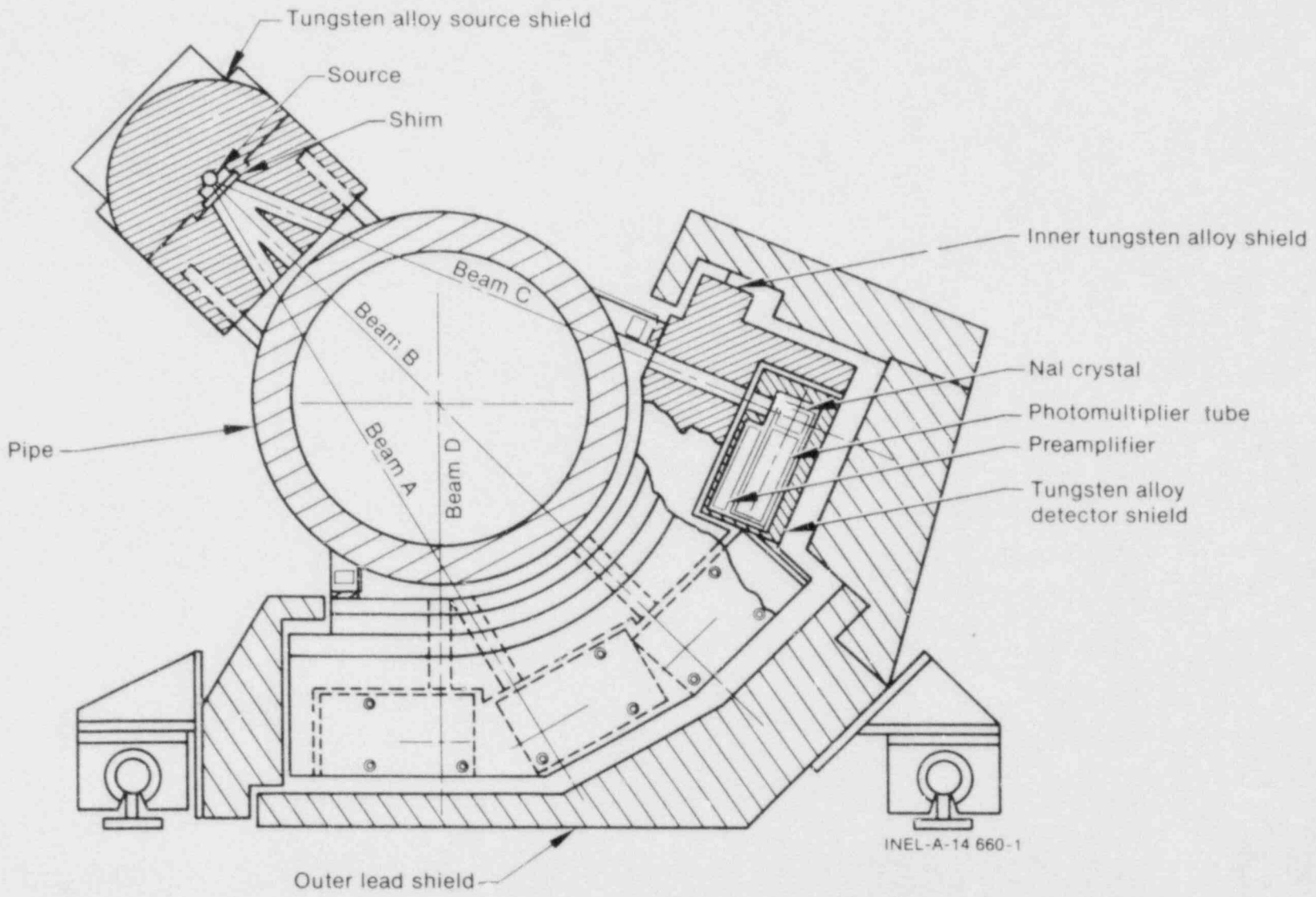

Figure 1. Densitometer mounted on pipe.

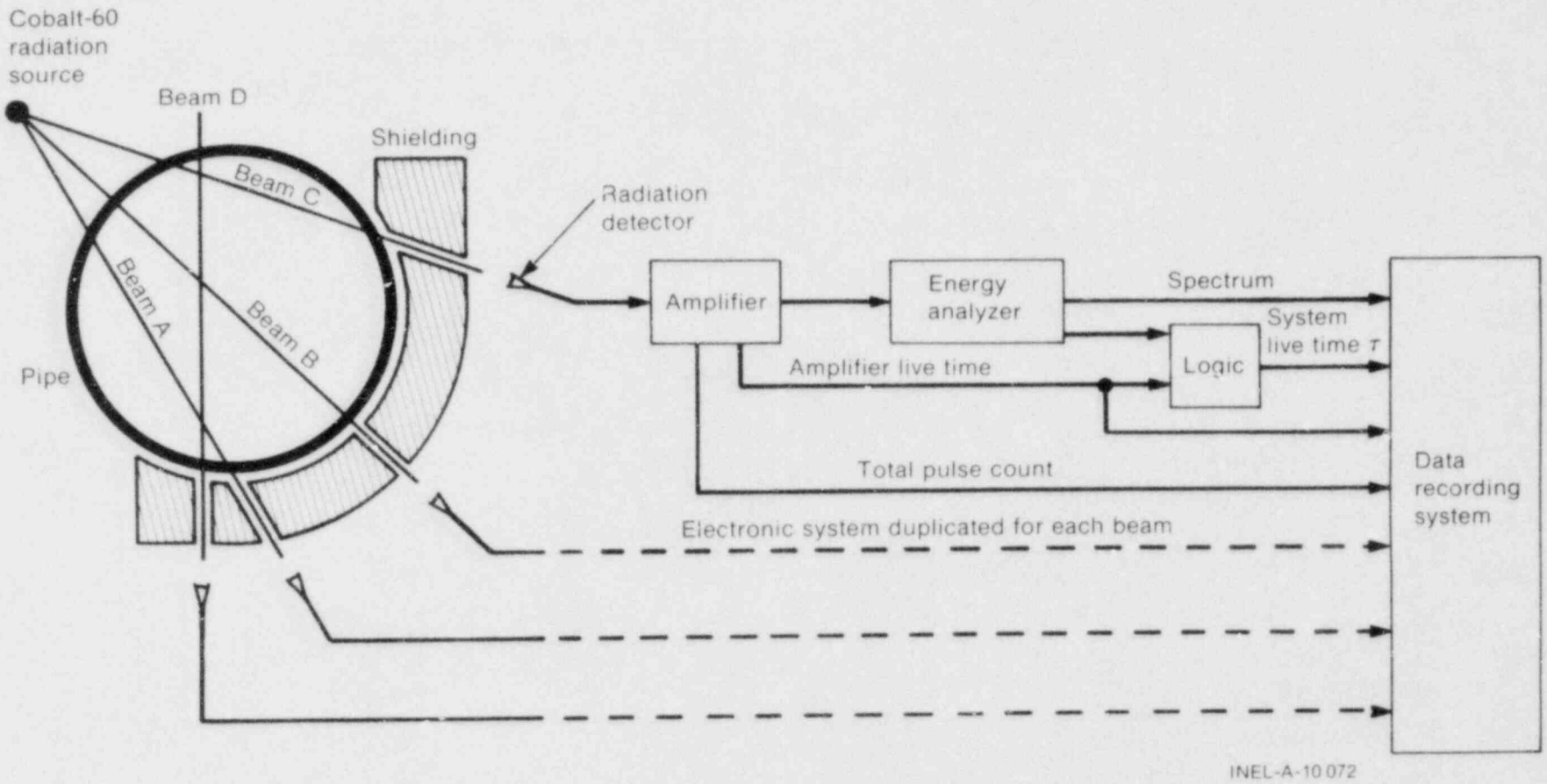

Figure 2. Schematic diagram of the electronics system hardware for the LOFT radiation-hardened densitometer.

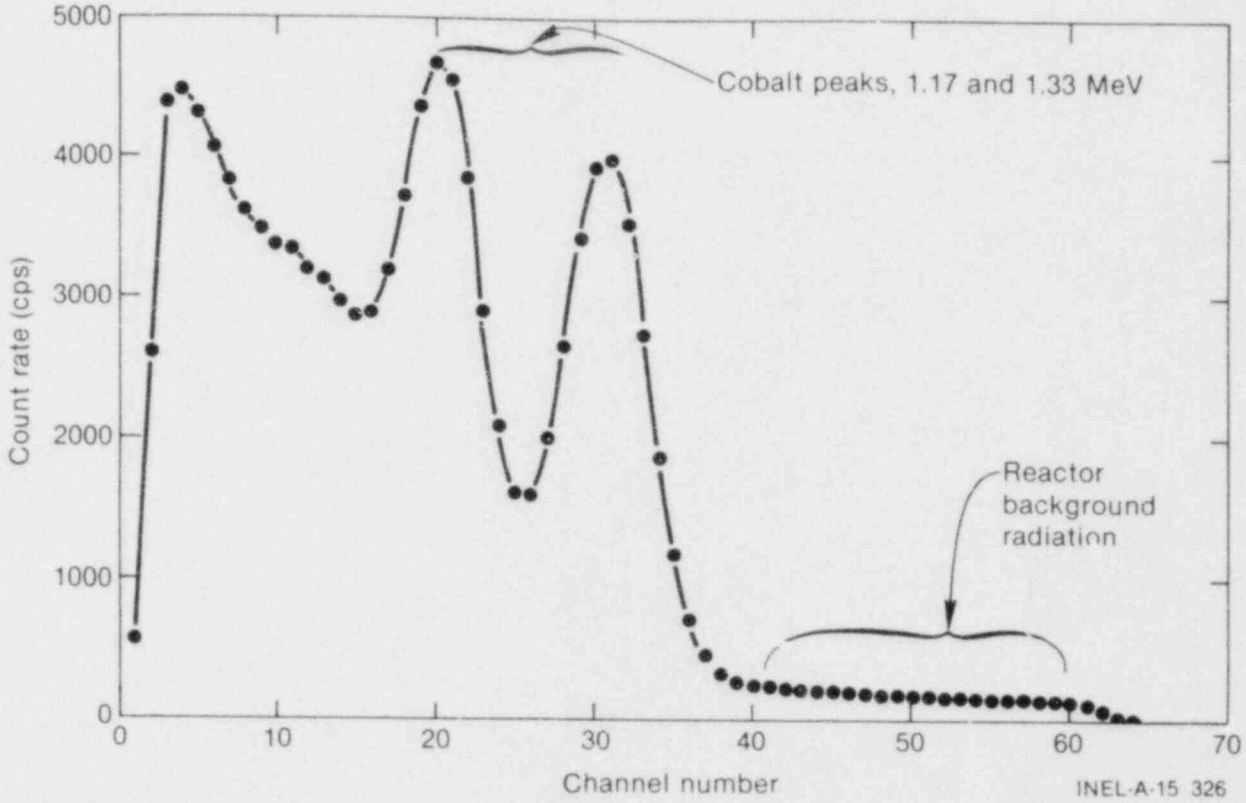

Figure 3. Raw pulse amplitude spectrum for Beam B representing a 100-second measurement period.

3. DATA ANALYSIS PROCEDURES

In the data analysis, two photon energy ranges (α and β) are selected by the analyst. The α range is chosen to include the two cobalt radiation peaks at 1.17 and 1.33 MeV. The β range is a higher energy range which includes little or no cobalt radiation. The α and β energy ranges correspond to α and β ranges in pulse amplitude spectrum channel number, since there is a linear relationship between channel number and absorbed photon energy. The α and β channel number ranges may be different for different beams, because the relationship between energy and channel number may be different for different beams. For the spectrum shown in Figure 3, for example, the α range might be channels 16 through 38 and the β range might be channels 40 through 60.

The recorded pulse amplitude spectrum for each beam is summed over each of the α and β ranges to produce two numbers, I_α and I_β. That is, I_α is the number of pulses detected in the α range during the measurement period. This gives five primary measured quantities (I_α, I_β, P', N', and N) for each beam for each measurement period.

The live time fractions τ and τ' are estimated from N and N' using

$$\tau = (N + 1)/(K + 2) \tag{1}$$

with the same equation for τ' and N', where K is the number of live time clock pulses generated (but not necessarily counted) during the measurement period. The dead-time-corrected count rates for the α and β ranges are estimated using

$$A'_\alpha = I_\alpha / (\tau T) \tag{2α}$$

and the β analog for the β range[a], where T is the length of the measurement period.

The photon energy absorption event rate P is estimated using

$$P = P'/(\tau' T). \tag{3}$$

The five primary measured quantities are thus replaced with three estimated ensemble average quantities (A'_α, A'_β, and P) for each beam for each time interval.

For Beam D, denoted hereafter by the subscript 4, the quantities $B_{\alpha 4}$ and $B_{\beta 4}$ are calculated using Equation (4)[b]:

$$B_{\alpha 4} = e^{P_4 R} A'_{\alpha 4}/P_4 - \left[1 - e^{-P_4 R}\right] F_{0\alpha 4} - \left[1 - e^{-P_4 R}\right]^2 G_{0\alpha 4} \tag{4α}$$

where R is a time that is characteristic of the electronics (nominally 125 ns) and the F and G quantities are determined from preliminary measurements.

The $B_{\alpha 4}$ and $B_{\beta 4}$ values obtained from Equation (4) are then smoothed over time to remove the high frequency fluctuations due to the randomness inherent in the radiation process. This smoothing is justified by the assumption that the shape of the background radiation spectrum should not change rapidly. The $B_{\alpha 4}$ and $B_{\beta 4}$ values are also corrected for the effects of radiation scattering from Beam A into Beam D.

---

a. Many equations in this discussion occur in pairs which are the same except for the α or β subscript. Usually only the α equation with the α subscript terms is written explicitly. The β analog can be obtained by simply replacing the α subscript with a β subscript.

b. Insert β subscript to calculate $B_{\beta 4}$.

Most of this scattering occurs in the steel pipe wall next to the detectors for Beams A and D. The correction is based on the assumption that the magnitude of the scattered radiation intensity is directly proportional to the intensity of the cobalt radiation detected in Beam A. The proportionality constant is determined from preliminary measurements with the cobalt source in the stored position and with the cobalt source in the exposed position (operating position).

Beam A, B, and C quantities are denoted by the subscripts 1, 2, and 3, which are represented in general by the subscript i. For each of Beams A, B, and C separately, an iterative procedure is used to solve for C_i from the equations

$$B_i \, B_{\alpha 4} + C_i \, C_{\alpha i} = A_{\alpha i} \tag{5α}$$

and

$$B_i \, B_{\beta 4} + C_i \, C_{\beta i} = A_{\beta i}, \tag{5β}$$

where $C_{\alpha i}$ and $C_{\beta i}$ are constants determined from preliminary measurements, B_i is an unknown, and $A_{\alpha i}$ and $A_{\beta i}$ are defined by Equation (6)[a]:

$$A_{\alpha i} = A'_{\alpha i} \, e^{P_i R} - \frac{(1 - e^{-P_i R})}{P_i} \left[B_i^2 \, F_{0\alpha i} + 2 \, B_i \, C_i \, F_{1\alpha i} + C_i^2 \, F_{2\alpha i} \right]$$

$$- \left[\frac{(1 - e^{-P_i R})}{P_i} \right]^2 \left[B_i^3 \, G_{0\alpha i} + 3 \, B_i^2 \, C_i \, G_{1\alpha i} \right.$$

$$\left. + 3 \, B_i \, C_i^2 \, G_{2\alpha i} + C_i^3 \, G_{3\alpha i} \right]. \tag{6α}$$

The C_i values are the calculated cobalt radiation beam intensity values used to calculate the chordal average density values:

$$\rho = a + b \ln C \tag{7}$$

where C is the C_i value determined for Beam i, ρ is the chordal average density, and a and b are calibration coefficients.

The calibration coefficients are different for different beams. They are calculated from

$$b = \frac{\rho_g - \rho_l}{\ln (C_g / C_l)} \tag{8}$$

and

$$a = \frac{\rho_l \ln (C_g) - \rho_g \ln (C_l)}{\ln (C_g / C_l)}, \tag{9}$$

---

a. Insert β subscript to calculate $A_{\beta i}$.

where the subscripts l and g refer to liquid and gas, respectively. C_l is the cobalt radiation beam intensity when the pipe is filled with liquid before the blowdown starts. ρ_l is the liquid density during that time, determined from pressure and temperature measurements and steam tables. C_g is the highest value on the smoothed curve of cobalt radiation beam intensity versus time. The pipe is assumed to be filled with gas at that time, and ρ_g, the density of that gas, is determined from temperature and pressure measurements for that time.

If no all-gas calibration point is available, the second calibration point is the point with the pipe full of liquid and with the shim inserted to attenuate the beams by some known amount. The effective density for this condition is greater than the liquid density instead of being very small as it is for an all-gas calibration.

Another alternative to the measured all-gas calibration point is the use of a theoretically calculated value of C_g in place of the missing measured value. The C_g value can be calculated from a measured C_l value and known parameters such as densitometer geometry and mass attenuation coefficients. The use of the calculated C_g value, in place of the measured C_g value, in the calibration procedure [Equations (8) and (9)] is equivalent to the more direct process of using a theoretically calculated value of b and using

$$\rho = \rho_l + b \ln (C/C_l) \tag{10}$$

in place of Equation (7).

While the reactor is running in steady state conditions before the blowdown starts, two 512-channel spectra are recorded for each beam: one spectrum with the cobalt source in the stored position, and the other with the cobalt source in the exposed position. These spectra are averaged over a long data acquisition time, to reduce to a negligible magnitude the uncertainty due to the randomness in the radiation process. These preliminary measurements are used to determine the spectrum shape coefficients (C_α, C_β, and the F and G coefficients) for each beam and, also, to determine the amount of scattering from Beam A into Beam D.

4. UNCERTAINTY ESTIMATES

The general procedure for estimating the measurement uncertainty, that is, the uncertainty in the calculated chordal average density values, is to estimate the uncertainty in the primary measured quantities and in the various parameters used in the data processing, and to calculate the effects of these several uncertainty sources on the final result, the calculated density values.

The following sections of this report contain a brief outline of the general mathematical techniques used for estimating uncertainty propagation; a list of important variables in this analysis; discussions of the several known, significant sources of uncertainty and their effects on the independent variables; a discussion of the propagation of these individual uncertainty contributions; and a summary of the overall effect of these uncertainties. In reading these sections, it may be helpful to refer occasionally to Table 1, which summarizes the uncertainty contributions to the important intermediate variable C (beam intensity).

In the following discussions, some potential uncertainty contributions are described as being removed by the calibration procedure. This is because the effects of certain types of errors in C disappear when C is converted to ρ, even though the errors in C may be very large. This is a result of the calibration procedure used in this measurement system, as is discussed in more detail in Section 4.17, "Uncertainty Propagation into ρ."

4.1 Uncertainty Propagation

The uncertainty in any quantity Z is characterized by σZ, the standard deviation in the values of Z in a hypothetical ensemble of replications of an experiment in which Z could be measured. Formally, σZ is defined by

$$\sigma Z = \left\{ u \left[(Z - \mu Z)^2 \right] \right\}^{1/2}, \tag{11}$$

where μZ is the ensemble average or mean value of Z. In practice, if Z is a dependent variable, the value of σZ is estimated by the common formula

$$\sigma Z = \left[\sum_i \left(\frac{dZ}{dX_i} \sigma X_i \right)^2 \right]^{1/2}, \tag{12}$$

where the X_i are independent variables and the sum is over all the independent variables. This procedure assumes that the dependence of Z on each X_i is approximately linear for X_i values within about $\pm 2\sigma X_i$ of the nominal value of X_i being considered.

If Z can be expressed in terms of some intermediate variables Y_j, such that no two of the Y_j depend on the same independent variable X_i and no Y_j depends on any X_i that appears explicitly in the expression for Z, then a very helpful concept, analogous to the chain rule in evaluating derivatives, results:

$$(\sigma Z)^2 = \sum_i \left(\frac{\partial Z}{\partial X_i} \sigma X_i \right)^2 + \sum_j \left(\frac{\partial Z}{\partial Y_j} \sigma Y_j \right)^2, \tag{13}$$

TABLE 1. CONTRIBUTIONS TO $\sigma C/C$

Error	X	$\sigma X/X$	$\lvert X/C\ dC/dX \rvert$	$\sigma C/C$ Contribution	Remarks
Random errors	τ	$\left[\frac{1-\tau}{(K+3)\tau}\right]^{1/2}$ <0.063	$\left\lvert e^{PR}(D_\beta A'_\alpha - D_\alpha A'_\beta)/C \right\rvert \approx 1$	<0.063	
	τ'	$\left[\frac{1-\tau'}{(K+3)\tau'}\right]^{1/2}$ <0.063	$\left\lvert RP(D_\beta A'_\alpha - D_\alpha A'_\beta)/C \right\rvert \approx RP < 0.09$	<0.0057	
	I_α	$1/\sqrt{I_\alpha}$	$- D_\beta A'_\alpha e^{PR}/C \approx A'_\alpha/(C_\alpha C)$,	$<\frac{1.3}{\sqrt{I_\alpha}}$	
			$<1.3,\ >1.0$	$\geq \frac{1.0}{\sqrt{I_\alpha}}$	Decreases as background decreases.
	I_β	$1/\sqrt{I_\beta}$	$\left\lvert - D_\alpha A'_\beta e^{PR}/C \right\rvert \approx B_{\alpha 4} A'_\beta/(B_{\beta 4} C_\alpha C)$	<0.11	Decreases to zero as background decreases.
	P'	$1/\sqrt{P'} < 0.035$	$RP(D_\alpha A'_\beta - D_\beta A'_\alpha)/C \approx RP < 0.09$	< 0.0032	
	B_α	0.0018	$\left\lvert D_\beta B_\alpha B/C \right\rvert \approx B_\alpha B/(C_\alpha C) < 0.3$	<0.0006	Band-limited noise.
	B_β	0.018	$- D_\alpha B_\beta B/C \approx B_\alpha B/(C_\alpha C) < 0.3$	<0.006	Band-limited noise.
Bias errors	R	<0.2	Effect on C is not calculated.		

TABLE 1. (continued)

Error	X	σX/X	|X/C dC/dX|	σC/C Contribution	Remarks
Bias errors	C_α	<0.1	$\left\|D_\beta C_\alpha\right\| \approx 1$	<0.1	Mostly removed by calibration procedure.
	C_β	<0.1	$-D_\alpha C_\beta$ <0.1	<0.01	Mostly removed by calibration procedure.
	$F_{0\alpha}$	<0.1	$\left\|F_{0\alpha} D_\beta RB^2/C\right\|$ <0.09 B/C	< 0.009	Mostly removed by calibration procedure.
	$F_{0\beta}$	<0.1	$-F_{0\beta} D_\alpha RB^2/C$ <0.09 B/C	< 0.009	Mostly removed by calibration procedure.
	$F_{1\alpha}$	<0.1	$\left\|F_{1\alpha} D_\beta 2\ RB\right\|$ <0.2	<0.02	Mostly removed by calibration procedure.
	$F_{1\beta}$	<0.1	$-F_{1\beta} D_\alpha 2\ RB$ <0.2	<0.02	Mostly removed by calibration procedure.
	$F_{2\alpha}$	<0.1	$\left\|F_{2\alpha} D_\beta RC\right\|$ <0.1	<0.01	Mostly removed by calibration procedure.

TABLE 1. (continued)

Error	X	σ X/X	|X/C dC/dX|	σ C/C Contribution	Remarks
Bias errors	$F_{2\beta}$	<0.1	$-F_{2\beta} D_\alpha RC$ <0.1	<0.01	Mostly removed by calibration procedure.
	$G_{0\alpha}$	<0.1	$\left\|G_{0\alpha} D_\beta R^2 B^3/C\right\|$ <0.01 B/C	<0.001	Mostly removed by calibration procedure.
	$G_{0\beta}$	<0.1	$G_{0\beta} D_\alpha R^2 B^3/C$ <0.01 B/C	<0.001	Mostly removed by calibration procedure.
	$G_{1\alpha}$	<0.1	$\left\|G_{1\alpha} D_\beta 3R^2 B^2\right\|$ <0.024	<0.0024	Mostly removed by calibration procedure.
	$G_{1\beta}$	<0.1	$-G_{1\beta} D_\alpha 3R^2 B^2$ <0.024	<0.0024	Mostly removed by calibration procedure.
	$G_{2\alpha}$	<0.1	$\left\|G_{2\alpha} D_\beta 3R^2 BC\right\|$ <0.024	<0.0024	Mostly removed by calibration procedure.
	$G_{2\beta}$	<0.1	$-G_{2\beta} D_\alpha 3R^2 BC$ <0.024	<0.0024	Mostly removed by calibration procedure.

TABLE 1. (continued)

Error	X	$\sigma X/X$	$\lvert X/C\ dC/dX \rvert$	$\sigma C/C$ Contribution	Remarks
Bias errors	$G_{3\alpha}$	<0.1	$\lvert G_{3\alpha} D_{\beta} R^2 C^2 \rvert$ <0.01	<0.001	Mostly removed by calibration procedure.
	$G_{3\beta}$	<0.1	$- G_{3\beta} D_{\alpha} R^2 C^2$ <0.01	<0.001	Mostly removed by calibration procedure.
				<0.02	Model uncertainty (pulse shape).
				<0.001	Polyenergetic gamma source radiation.
				<0.019	Scattering.
				<0.01	Thermal expansion.
Other errors	B_{α}			<0.03, 0.05, and 0.02	For Beams A, B, and C, respectively. Beam A to Beam D scattering when density and background radiation are small.

where

$$(\sigma Y_j)^2 = \sum_i \left(\frac{dY_j}{dX_i} \sigma X_i \right)^2 . \qquad (14)$$

These equations imply that, if the above-stated conditions are met, the uncertainties in intermediate variables can be estimated from the uncertainties in the independent variables from Equation (14), and then the intermediate variables can be treated as independent variables in the next step of the uncertainty propagation analysis, Equation (13). Proceeding thus in steps is often much simpler than doing the entire analysis in one large, complicated step.

4.2 Important Variables

In this uncertainty analysis, the final dependent variables (analogous to the Z just discussed) are ρ_i, i = 1, 2, and 3, which are the calculated chordal average density values for densitometer Beams A, B, and C, respectively. The quantities $I_{\alpha i}$, $I_{\beta i}$, P'_i, N'_i, N_i, $B_{\alpha 4}$, $B_{\beta 4}$, $C_{\alpha i}$, $C_{\beta i}$, ρ_{li}, ρ_{gi}, and R and the 14 F and G coefficients for each of the three beams, can be taken as independent variables [the X's in Equations (11) through (14)]. Some useful intermediate variables [the Y's in Equations (13) and (14)] are B_i, C_i, P_i, τ_i, τ_i, $A'_{\alpha i}$, and $A'_{\beta i}$.

Instead of I_α and I_β, the individual spectrum elements that are summed to obtain I_α and I_β could be used as independent variables. However, such a choice would greatly increase the complexity of the analysis without giving any different, useful information.

C_α, C_β, and the F and G coefficients are not actually raw measurements, but are derived from analyses of data acquired before the blowdown experiment s[illegible] strictly proper procedure would be to study in detail the propagation of uncertainties from the [illegible]urements into the values of C_α, C_β, and the F,and G coefficients, rather than treating C_α, C_β, . . .nd G as independent variables. However, as shown later, the contributions of the C_α, C_β, F, and G uncertainties to the final overall measurement uncertainty are relatively small, and the detailed study of these uncertainty contributions seems unwarranted.

4.3 Radiation Process Randomness

A major source of uncertainty in the LOFT radiation-hardened densitometer is the randomness inherent in the radiation process. This randomness is manifest as two types of uncertainties in the LOFT densitometer: an uncertainty in the estimate of the ensemble average of the number of detected photon pulses, and an uncertainty in the estimate of each of the live time fractions.

4.3.1 Live Time Uncertainty. Since the detected photon pulses occur at random times, any one photon pulse may or may not fall on a live time clock pulse and contribute to the measured dead time. Therefore, a single observed value of N, the number of live time clock pulses counted while the system is live, may result from different values of the live time fraction τ, depending on whether more or fewer photon pulses happen to fall on live time clock pulses.

If τ is completely unknown before the experiment and N live time clock pulses are counted during the experiment, the best estimate of τ after the experiment is

$$\tau = (N + 1)/(K + 2), \qquad (15)$$

and the standard deviation of this estimate is

$$\sigma\tau = \left[\frac{(N+1)(K-N+1)}{(K+2)^2(K+3)}\right]^{1/2} = \left[\frac{\tau(1-\tau)}{K+3}\right]^{1/2} \quad (16)$$

where K is the number of live time pulses generated (but not necessarily counted) during the measurement period, and the value of τ on the right side of Equation (16) is that value calculated in Equation (15).

The uncertainty described by Equation (16) is random noise in the calculated value of τ. The term "random noise," as used here and later in this report, means an error that is completely independent (uncorrelated) from one data point or data frame to the next. This type of error appears as a white noise contribution in a graph of the variable (τ in this case) versus time.

For the LOFT densitometer with the 20-kHz live time clock and the normal 12.5-ms measurement period, K = 250 and

$$\frac{\sigma\tau}{\tau} = \left[\frac{1-\tau}{253\,\tau}\right]^{1/2} . \quad (17)$$

If the effective measurement period is increased by adding or averaging several 12.5-ms frames, then the values of N and K in Equations (15) and (16) are the sums of the values for the several frames included in the average.

For LOFT Loss-of-Coolant Experiments (LOCEs) L2-2[3], L2-3[4], and L3-0[5], the traditional

$$\tau = N/K \quad (18)$$

was used instead of Equation (15). Equation (18) introduces a bias in the τ estimate. For these experiments, τ was between 0.5 and 1.0, which implies that the error in τ resulting from the use of Equation (18) was smaller than 1/K or 0.004. The densitometer calibration procedure removes a large part of this error, leaving a live time induced bias error in the density computation which is zero at both ends of the density range and is less than 1.2 kg/m^3 for the worst beam (Beam C) in the middle of the density range. The bias error is less than 0.6 kg/m^3 for Beam A. This bias error will not occur for experiments conducted after LOCE L3-0.

All of the preceding discussion on τ is equally applicable to τ', except that the final effect of the bias error in τ' is only about one tenth as large as that due to τ.

No other significant uncertainty contributions are known for τ and τ'. Therefore, neglecting the bias error in the uncertainties for LOCEs L2-2, L2-3, and L3-0, the uncertainty in τ is a random noise with root-mean-square magnitude given by Equation (16). τ' has exactly the same type of uncertainty.

4.3.2 Ensemble Average Pulse Count Uncertainty. The fluid density is related to the expected value (the ensemble average) of the intensity of the cobalt radiation that is transmitted through the fluid, which is obtained from the ensemble average of the number of photon pulses counted during the experiment. This ensemble average number of pulses is never measured. The measured quantity is the number of pulses counted during one particular experiment, which may vary from one trial to the next even though the fluid density and all other macroscopic parameters are held exactly constant. The best estimate of the desired ensemble average number of pulses is simply the measured number of pulses, and the standard deviation of this estimate is the square root of the ensemble average value. Thus, the measured values of I_α, I_β, and P' are also the estimated ensemble average values to be used in the calculations, and the estimated standard deviations are

$$\sigma I_\alpha = \sqrt{I_\alpha} , \tag{19α}$$

$$\sigma I_\beta = \sqrt{I_\beta} , \tag{19β}$$

and

$$\sigma P'_s = \sqrt{P'} . \tag{20}$$

The uncertainties represented by Equations (19) and (20) appear as random noise in I_α, I_β, and P'. This is the only known, significant uncertainty in I_α and I_β, but P' has an additional uncertainty contribution due to a truncation, which is discussed shortly.

For Beams A, B, and C, Equations (19) and (20) are directly usable representations of the statistical uncertainty. For Beam D, the effect of this uncertainty is rather indirect; it is discussed in Section 4.9.

4.3.3 Coincidence Correction Uncertainty. The coincidence correction is a mathematical correction applied to account for those pulse pile-up events that are not rejected by the electronics. Because pulse pile-up events occur randomly, it might be argued that the coincidence correction has an uncertainty similar to that in the estimated ensemble average of the number of counts (as discussed in the previous section). This argument might be valid when trying to correct the measured spectrum. However, the philosophy used here is to apply the coincidence correction to the (estimated) ensemble average spectrum. (In fact, it appears to be impossible to apply this or any similar correction without assuming that the spectrum is the ensemble average.) When applying the coincidence correction to the ensemble average quantities, there is no introduction of additional error due to the randomness of the radiation processes. (Of course, the uncertainties already present in τ, τ', I_α, I_β, and P' are propagated through the mathematical manipulations in the coincidence correction and contribute to the uncertainty in the final results.)

4.4 Truncation of P′

The least significant five bits of the P' values are truncated before P' is recorded. This process is equivalent to dividing P' by 32 and discarding the fractional part of the quotient. During the data processing, the recorded value is multiplied by 32, but there is no way to restore the discarded part of the P' value exactly. The bias error in P' can be removed by restoring the average value of the discarded part (15.5), but there remains a random uncertainty corresponding to the difference between 15.5 and the actual value of the discarded part of P'. Assuming that the actual discarded values are uniformly distributed over the range from 0 to 31 (as was already done in determining the average of 15.5), the standard deviation of the discarded values, and hence the root-mean-square error due to this truncation process, is

$$\sigma P'_t = 9.233. \tag{21}$$

The total uncertainty in P' is the root-sum-square of the two components represented by Equations (20) and (21):

$$\sigma P' = \left[(\sigma P'_s)^2 + (\sigma P'_t)^2 \right]^{1/2} = \left[P' + 85.25 \right]^{1/2} . \tag{22}$$

The truncation uncertainty becomes insignificant (less than 5% of the total P′ uncertainty) for P′ values greater than 832, which corresponds to a total count rate of about 67 000 photons per second. This count rate is below the lowest count rates observed, so it is reasonable to represent the total uncertainty in P′ by the statistical uncertainty alone (Equation 20), as long as the densitometer system is used in the normal mode with the sources exposed. If the densitometer sources are stored, the count rate may drop well below 67 000 and the truncation error may become significant. This abnormal circumstance is not considered further.

4.5 Variations in R

R is the time required for the electronic pulse, representing a photon detection event, to rise from zero to its peak value. R is nominally 125 ns, but variations in electronic components, as well as drift due to temperature variations or aging, could cause significant variations from one beam to another and also variations with time for a single beam.

The uncertainty associated with these variations in R is not treated the same way as the uncertainties associated with the other variables, because the mathematical propagation of this particular uncertainty component through all the equations is very cumbersome. Rather, estimates of the effects of the uncertainty due to R variations are based on observations.

Several sets of data have been processed both with and without the coincidence correction, which is the same as using R = 125 ns and R = 0. The largest calculated density change associated with this 100% change in the R value was 32 kg/m^3. Although R does not enter linearly into the equations, the calibration procedure tends to make the final effect of R variations approximately linear, and it seems reasonable to assume that a 20% change in R should cause a change no larger than about 6.4 kg/m^3 in the calculated density values. It is assumed here that ± 20% is a reasonable upper bound for variations in R, and that ± 6.4 kg/m^3 is therefore a reasonable upper bound on the final uncertainty contribution due to R variations. This value is for Beam B, which has the highest total photon count rate. The corresponding uncertainty in Beams A and C should be roughly ± 4.0 kg/m^3 and ± 2.5 kg/m^3, respectively, assuming that the uncertainty in the calculated ρ values is proportional to the total photon count rate. These uncertainty values apply only near the middle of the density range; this uncertainty component decreases to zero as ρ approaches either ρ_l or ρ_g, because this type of systematic error is mostly removed by the calibration procedure.

4.6 Spectrum Shape Coefficients

A set of 16 coefficients (C_α, C_β, and 14 F and G coefficients) are needed for each of Beams A, B, and C, and 4 coefficients ($F_{0\alpha}$, $F_{0\beta}$, $G_{0\alpha}$, and $G_{0\beta}$) are needed for Beam D. These coefficients describe certain important features of the shape of the spectrum for each beam. They are derived from preliminary data that are recorded before the experiment. The calculations depend mainly on the general shapes of the preliminary spectra, with very little dependence on the spectrum magnitudes, details of the spectrum shapes, count rates, live times, or other parameters that are important in the routine data processing. The spectra used in these calculations are averaged over a long time, typically 20 or 30 seconds, so that statistical variations in the general shape of each spectrum are negligible. The calculations are done by an iterative procedure which converges very quickly and is expected to introduce errors not larger than 1% of the calculated values. In short, the calculated spectrum shape coefficients should have uncertainties much less than 10% of the calculated values. Thus,

$$\frac{\sigma X}{X} < 0.1 \qquad (23)$$

is assumed, where X is any one of the spectrum shape coefficients.

4.7 Beam A to Beam D Scattering

Beam A and Beam D intersect at the bottom of the pipe where Beam A is leaving the pipe, close to the detectors for Beams A and D. The pipe metal in this region of intersection scatters a measurable amount of the cobalt radiation from Beam A into the Beam D detector. This scattered radiation appears in the α range of the Beam D spectrum, and it adds a bias error to the B_α value calculated from the Beam D spectrum. This bias error is not important when there is a lot of background radiation or when Beam A is strongly attenuated by high-density fluid in the pipe. However, for low fluid density and low background radiation conditions, this error in B_α can dramatically affect the calculated chordal average density for Beams A, B, and C.

In principle, this bias error can be removed during the data analysis, using correction coefficients calculated from the preliminary data. However, the scattered radiation is hardly observable in the preliminary data, and the calculated correction coefficients are of questionable accuracy. The analysis procedure includes a feature that limits the B_α values to a reasonable range and, thereby, limits the effect of the bias error. However, some error can still occur.

There is some indication, although the evidence is not conclusive, that this error in B_α may cause errors as large as 5% in the calculated value of C for Beam B. The magnitude of the effect on C is believed to be approximately proportional to P, which suggests errors as large as 3% for Beam A and 2% for Beam C. These values are taken as the best estimate of the worst case effects of the scattering error.

This error in the C value is very likely to occur when the C value is at or near its maximum for an experiment, so that there is a good chance that the most erroneous value of C is used as C_g in the calibration procedure. This would cause the error to be spread throughout the entire set of ρ values, instead of being limited to those points in which there actually was a bias error in B_α. In this case, the errors in ρ would gradually decrease to zero as ρ approached ρ_l, but there could be significant errors for ρ near ρ_g. The use of bad C values for C_g can probably be avoided in most cases by checking for the presence of scattered cobalt radiation peaks in the Beam D spectra representing the suspect time intervals.

The magnitude of the error due to scattering from Beam A to Beam D is strongly dependent on errors in the assumed location of the α range in the Beam D spectra. If the specified α range of channel numbers is lower than the correct α range, a larger amount of scattered radiation is included in the α range and the error in the calculated B_α value is greater. (This problem of knowing the correct α range position is discussed further in Section 4.8.) The previously quoted error bounds of 5, 3, and 2% (of the calculated C value), for Beams B, A, and C, respectively, include the effects of uncertainty in the α range position.

4.8 Beam D Energy Calibration

The spectra for Beam D are used to determine the shape of the background radiation spectra, and this information (in the form of B_α and B_β) is used in the background subtraction in analyzing the data for Beams A, B, and C. This procedure demands that all four α ranges of channel numbers (for all four beams) represent the same photon energy range, and that all four β ranges of channel numbers represent the same energy range. It is easy to determine the relationship between channel number and photon energy for Beams A, B, and C, because the easily identifiable cobalt peaks provide two calibration points. Beam D, however, does not always have such an unambiguous calibration, and there is some uncertainty about which channel numbers should be assigned to the α and β ranges.

Usually, as long as the ratio of B_α to B_β is correct, the absolute magnitudes of B_α and B_β are not very important. When the background radiation levels are high, the background spectrum is approximately an exponential function of energy in the region near the cobalt peaks, and the ratio of B_α to B_β is insensitive

to errors in energy calibration or placement of the α and β ranges. However, when the background radiation from the nuclear reactor dies down and cobalt radiation accounts for a significant part of the Beam D spectrum, large errors in B_α/B_β, and in C, can result from errors in the α range and β range placement. The error in C is limited by restricting the value of B_α/B_β to a reasonable range, but even with this limit, the errors in C may approach 3, 5, and 2% for Beams A, B, and C, respectively. This is the same uncertainty contribution that was mentioned in the discussion of Beam A to Beam D scattering, not a separate, additional contribution. That is, the 3, 5, and 2% uncertainties represent the combined effects of Beam A to Beam D scattering and Beam D energy calibration uncertainty. The uncertainty associated with each of these effects separately is not known.

4.9 Radiation Process Randomness in B_α and B_β

The quantities B_α and B_β are approximately proportional to the numbers of counts in the α range and the β range, respectively, of the Beam D spectrum. The number of counts in the β range may be as low as 25, which implies a standard deviation of 20% in the raw (unsmoothed) B_β value. This uncertainty is associated with the randomness in the radiation processes and appears as a random noise component in the raw B_β values. The standard deviation in B_α is only about 2%, because the α range has a minimum count rate greater by a factor of at least 100 than the minimum count rate in the β range.

The raw B_α versus time and B_β versus time curves are both smoothed by two applications of a moving average filter; one with 99 points and one with 79 points in the window. This smoothing reduces the random noise amplitude by a factor of about 0.085. The smoothing also limits the bandwidth of the noise, so it is no longer "white" but has only low-frequency components. That is, the error in any data point is correlated with the errors in nearby (in time) data points.

Other potential sources of uncertainty in B_α and B_β, such as uncertainty in the total count rate for Beam D or uncertainties in the calculation procedures or parameter values, are negligible compared with the uncertainties already discussed. Therefore, the uncertainties assigned to B_α and B_β are:

1. Band-limited random noise, with

$$\sigma B_\alpha/B_\alpha = 0.0018 \qquad (24\alpha)$$

and

$$\sigma B_\beta/B_\beta = 0.018. \qquad (24\beta)$$

2. A combination of scattering and energy calibration errors that cause uncertainties in the calculated beam intensity C of magnitudes: (a) 3% for Beam A, (b) 5% for Beam B, and (c) 2% for Beam C, when the background radiation levels are low.

4.10 Gain Shift

The gain of the detector or the electronics sometimes changes during an experiment primarily because the gains are sensitive to the total count rate. Drifts of more than four channels have been observed in the worst cases. This corresponds to about four tenths of the difference between the two cobalt peaks, or about a 4% change in the apparent energy of the cobalt peaks. Such a drift can cause errors of about 15% in the calculated beam intensity, although a large part of this error is removed by the calibration procedure in some cases.

In response to this observed gain drift, the data processing programs were modified so that they compensate for gain changes. The programs effectively lock onto the cobalt peaks and follow them as they move to

different channel numbers in the recorded spectra during the course of the experiment. However, this drift compensation feature is not perfect, because of the previously mentioned radiation process randomness. Ideally, the drift compensation should be very fast, so that it responds promptly to a gain change. This means that the spectra that the program examines to find out where the cobalt peaks are, cannot be averaged over a long time. Therefore, the spectra have significant statistical fluctuations, and the calculated gain shift also has significant fluctuations. There is a trade-off between the speed and the accuracy of the drift compensation feature.

Tests with data recorded while the pipe was filled with cold liquid water indicate that the drift compensation feature greatly increases the random noise in C if the spectrum averaging time is the minimum value of 12.5 ms. If the averaging time is increased to 200 ms, the drift compensation does not significantly increase the noise in C. A 200-ms response time for drift compensation is usually acceptable, so it is assumed that the drift compensation procedure removes slow drift errors and does not introduce significant random errors. If a 200-ms averaging time is not allowed, the drift compensation should not be used, and there is an additional uncertainty component due to drift.

4.11 Model Uncertainty

The data analysis procedure includes a coincidence correction, a correction for pile-up pulses that are not rejected by the electronics. The F and G coefficients and the exponential factors in Equations (4) and (6) are associated with this coincidence correction. This correction is based on some assumptions about the shape of the electronic pulses output by the detector, and these assumptions are not entirely accurate. These inaccurate assumptions result in an incomplete correction for coincidence events. Analysis of a special set of test data suggests that the coincidence correction leaves a residual coincidence effect of not more than 2% in the calculated value of the beam intensity C. (The error in the calculated C value without the coincidence correction was 13% in this test data.) Although the residual errors in the densitometer data processing are expected to be smaller than those in the test data, the value of 2% is used as the upper bound of the uncertainty in C due to model inaccuracy. This error is negligible compared with the errors in the spectrum shape coefficients.

4.12 Polyenergetic Gamma Radiation

The logarithmic relationship shown in Equation (7) between beam intensity and density is theoretically valid only if all the radiation has the same mass attenuation coefficient. However, the radiation used in this densitometer system is approximately equally divided between two energies (1.17 and 1.33 MeV cobalt-60 radiation) for which the mass attenuation coefficients in water are approximately 0.065 and 0.060 cm^2/g. Using Equation (7) and the previously described calibration procedure for this densitometer is the same as approximating the actual (nonlogarithmic) beam intensity-density relationship with a logarithmic relationship that is exactly correct at the two calibration points. The worst error in this tacit approximation is equivalent to an error less than 0.1% in the beam intensity, which is negligible compared with previously-mentioned bias errors.

4.13 Miscellaneous Scattering Effects

Except for (a) the previously-discussed Beam A to Beam D scattering, and (b) small-angle scattering in the fluid, the effects of radiation scattering in the fluid and in the metal are expected to be well within the bounds specified for the previous (not radiation-hardened) densitometer. The total effect of these various scattering processes is estimated to be less than a 1.9% uncertainty in the beam intensity C. The effects of small-angle scattering were reconsidered for this densitometer. To a good approximation, small-angle scattering gives a measured beam intensity equal to $(1 + g\rho)$ multiplied by the correct, unscattered beam

intensity, where ρ is the chordal average fluid density and g is less than 0.004 for this densitometer. This type of error in C is almost completely removed by the calibration procedure, and the residual effect is negligible. Therefore, 1.9% of C is used as the upper bound estimate for all uncertainties introduced by scattering, excluding the previously-discussed Beam A to Beam D scattering.

4.14 Pipe Thermal Expansion

If the entire pipe and densitometer assembly expand at the same rate, the only effect is an increase in the length of the radiation beam path through the fluid. If the fluid is cold liquid water (the worst case), this effect produces a beam intensity decrease of about 0.003% per kelvin of rise in the pipe metal temperature. This effect is negligible, even for changes of 100 K which may occur during reflood.

A larger effect could occur if the pipe temperature changes, but the densitometer assembly temperature stays constant. If the pipe expands while the beam size remains fixed, some of the pipe metal moves out of the beam and the measured beam intensity rises. For Beam B, this effect should produce about an 0.08% increase in the measured beam intensity for a 1-K pipe temperature rise.

Pipe metal temperature and densitometer metal temperature measurements are not available, so the total magnitude of this effect is difficult to predict. However, existing data show that beam intensity changes are less than 1% when the fluid temperature changes by ~100 K in less than 50 seconds. This 1% value is used as the estimate of the maximum uncertainty in C due to thermal expansion effects.

4.15 Uncertainty Propagation into C

All of the previously discussed (Sections 4.3 through 4.14) uncertainty components contribute to the uncertainty in the intermediate variable C (the calculated beam intensity). Some of the uncertainty components are already specified in terms of ρ or C; for others, an uncertainty propagation analysis is required to determine the contribution to σC. For this analysis, Equation (14) is modified to give the more useful $\sigma C/C$ instead of σC:

$$\left(\frac{\sigma C}{C}\right)^2 = \sum \left(\frac{X}{C}\frac{dC}{dX}\right)^2 \left(\frac{\sigma X}{X}\right)^2 , \tag{25}$$

where X represents any one of the previously discussed independent variables and the sum is over all of those X's.

The derivative of C with respect to X can be obtained by taking the derivative of each of Equations (5α) and (5β) and algebraically eliminating dB/dX from the two resulting equations. The derivative of Equation (5α) is

$$\frac{dB}{dX} B_{\alpha 4} + B \frac{dB_{\alpha 4}}{dX} + \frac{dC}{dX} C_\alpha + C \frac{dC_\alpha}{dX} = \frac{\delta A_\alpha}{\delta X} + \frac{\partial A_\alpha}{\partial B}\frac{dB}{dX} + \frac{\partial A_\alpha}{\partial C}\frac{dC}{dX} \tag{26α}$$

which can be rearranged to give

$$\frac{dB}{dX}\left[B_{\alpha 4} - \frac{\partial A_\alpha}{\partial B}\right] + \frac{dC}{dX}\left[C_\alpha - \frac{\partial A_\alpha}{\partial C}\right] = \frac{\delta A_\alpha}{\delta X} - B\frac{dB_{\alpha 4}}{dX} - C\frac{dC_\alpha}{dX} , \tag{27α}$$

where the notation $\delta A_\alpha / \delta X$ is used here to denote the derivative with B and C held constant. In Equation (27α), and in its β analog, A_α and A_β are defined by Equation (6α) and its β analog. The derivatives of A_α and A_β can be evaluated for a particular X by referring to Equations (1), (2), (3), and (6). The derivatives of $B_{\alpha 4}$, C_α, and their β analogs are trivially evaluated for any given X. For example, dC_α/dX is 1 if X is C_α, or 0 if X is not C_α. Therefore, Equation (27α) and its β analog can be regarded as two linear algebraic equations in two unknowns, dB/dX and dC/dX, and these two equations can easily be solved for the desired dC/dX:

$$\frac{dC}{dX} = D_\alpha \left[\frac{\delta A_\beta}{\delta X} - B \frac{dB_{\beta 4}}{dX} - C \frac{dC_\beta}{dX} \right] - D_\beta \left[\frac{\delta A_\alpha}{\delta X} - B \frac{dB_{\alpha 4}}{dX} - C \frac{dC_\alpha}{dX} \right] , \tag{28}$$

where

$$D_\alpha = \left[B_{\alpha 4} - \frac{\partial A_\alpha}{\partial B} \right] \Big/ \text{DET} \tag{29α}$$

$$D_\beta = \left[B_{\beta 4} - \frac{\partial A_\beta}{\partial B} \right] \Big/ \text{DET} \tag{29β}$$

$$\text{DET} = \left[B_{\alpha 4} - \frac{\partial A_\alpha}{\partial B} \right] \left[C_\beta - \frac{\partial A_\beta}{\partial C} \right] - \left[B_{\beta 4} - \frac{\partial A_\beta}{\partial B} \right] \left[C_\alpha - \frac{\partial A_\alpha}{\partial C} \right] . \tag{30}$$

D_α, D_β, and DET do not depend on which variable X represents.

It is helpful to note some typical values and some limits on values for some of the parameters as follows:

1. R is nominally 0.125×10^{-6} second
2. $P < 0.7 \times 10^{6}$ seconds^{-1}
3. $B < P$
4. $C < P$
5. $F < 0.2$ for any subscripts
6. $G < 0.2$ for any subscripts
7. $B_{\alpha 4}$, $B_{\beta 4}$, and C_α are typically between 0.1 and 0.3
8. $C_\beta < 0.01$.

Using these values, the previously mentioned partial derivatives can be simplified by approximations to give

$$D_\alpha \approx -B_{\alpha 4}/B_{\beta 4}\ C_\alpha \tag{31α}$$

and

$$D_\beta \approx -1/C_\alpha . \tag{31β}$$

In addition to the already-discussed uncertainty estimators $\sigma X/X$ for the various independent variables X, Table 1 gives approximate expressions for the fractional derivatives (X/C) (dC/dX) and values for $|X/C\ dC/dX|\ \sigma X/X$ for each X.

The dominant random error contribution in Table 1 is that associated with I_α. The minimum magnitude of this term is $1/\sqrt{I_\alpha}$; it may be 50% higher when the background radiation intensity is high.

The minimum value of I_α is about 30. This value represents Beam C with the pipe full of cold water, with no background radiation, and with a 12.5-ms data acquisition period. I_α is about twice as large for Beam A or B. With the pipe empty, I_α values are about 350 for Beam A or B and about 100 for Beam C. These values vary with time as the source decays, and they depend substantially on the properties of the particular detector used.

Combining the $\sigma C/C$ contributions in Table 1 in the usual root-sum-square manner [in accordance with Equation (25)] gives the values of Table 2 for the total random, bias, and other uncertainty components in C. The different values for the random component result from the different values of I_α, as just discussed. Table 2 summarizes the effects of all the uncertainty sources already discussed except for the uncertainty in R.

TABLE 2. $\sigma C/C$ SUMMARY

Error	Beam A	Beam B	Beam C
Random error:			
Pipe empty, no background	0.14	0.14	0.16
Pipe full of cold liquid, maximum background	0.21	0.21	0.27
Bias error	0.11	0.11	0.11
Other errors (scattering from Beam A to Beam D)	0.03	0.05	0.02

4.16 Calibration Density Uncertainty

All the known, significant sources of uncertainty in ρ have been discussed except for the uncertainties in ρ_l and ρ_g, the densities used as calibration points. ρ_l and ρ_g are determined from temperature and pressure measurements with the assumption that the pipe is full of liquid or gas, respectively, when the temperature and pressure data are recorded. This assumption is expected to be valid for the liquid data point, and the standard deviation for the ρ_l value obtained from the steam tables is estimated to be 0.006 Mg/m^3.

The standard deviation of the ρ_g value obtained from the steam tables is estimated to be about 0.001 Mg/m^3, but the assumption that the pipe is filled with steam is sometimes questionable. Wet pipe walls could cause a bias error of 0.001 Mg/m^3 in ρ_g. If the pipe is filled with a mist instead of dry gas, the bias error could be substantially larger than 0.001 Mg/m^3. Worst of all, if there is liquid in the bottom of the pipe, the bias error could be several tenths of the liquid density. Unfortunately, there is no way to quantitatively predict this error, although it may be possible to estimate its magnitude in specific cases by comparing several beam readings or by using instruments other than the densitometer. If this possibility of liquid in the bottom of the pipe is neglected, minimum values are estimated as

$$\sigma\rho_g = 0.001 \text{ Mg/m}^3 \tag{32}$$

and

$$\sigma\rho_l = 0.006 \text{ Mg/m}^3. \tag{33}$$

The effect of errors in ρ_l and ρ_g is an offset error in ρ, with the magnitude of the offset depending on ρ. The effect of an error in ρ_g, for example, decreases linearly with ρ and is zero at $\rho = \rho_l$.

If the shim calibration procedure is used (because the all-gas data point is not available), then the value of ρ_g is not the actual gas density. Instead, it is the liquid density ρ_l plus the effective density of the shim, as listed in Table 3. The estimated uncertainty in this ρ_g value is represented by

$$\sigma\rho_g = 0.02 \text{ Mg/m}^3 \tag{34}$$

for the shim calibration procedure. This shim density uncertainty gives a measurement uncertainty contribution of $\sigma\rho = 0.14$ Mg/m^3 in the worst case. Because of this large uncertainty, the shim calibration should not be used except as a last resort. (It has not been used in any data reported to date.)

The other alternative to a measured all-gas calibration point is the use of theoretical b values in Equation (10). The theoretical b values, listed in Table 3, are within 5% of b values determined from data with reliably measured calibration points. Therefore,

$$\frac{\sigma b}{b} = 0.05 \tag{35}$$

is used as the estimate of the uncertainty in the theoretical b values.

TABLE 3. CALIBRATION DATA

Calibration Variables	Beam A	Beam B	Beam C
Effective density of shim (Mg/m^3)	0.1631	0.1367	0.2298
Theoretical value of b (Mg/m^3)	-0.65	-0.56	-0.88

4.17 Uncertainty Propagation into ρ

Equations (7), (8), and (9) can be combined to give

$$\rho = \frac{\rho_l \ln (C_g/C) + \rho_g \ln (C/C_l)}{\ln (C_g/C_l)} . \tag{36}$$

Equation (36) should be regarded as relating the dependent variable, ρ, to three independent variables, ρ_l, ρ_g, and C. C_l and C_g are not independent in the statistical sense. In fact, they are simply two particular values of C for certain times or fluid conditions.

This relationship between C, C_l, and C_g and the manner in which these three quantities appear in Equation (36) are a reflection of the tremendous advantage of the calibration procedure used with the LOFT radiation-hardened densitometer as compared with measurement systems in which the densitometer is not calibrated for each test separately. The advantage is that certain bias errors that may occur in C, also occur in C_l and C_g, and these errors cancel out in Equation (36). Thus, the calculated density ρ is relatively immune to bias errors in C, because the calibration procedure tends to remove bias errors. Specifically, if the calculated value of C is equal to a constant multiplied by the correct value of C, this error is completely removed in the calibration procedure. Other bias errors in C, such as the erroneous addition of a constant, are completely removed at $C = C_l$ and $C = C_g$, and they are usually greatly reduced for other values of C. For the bias errors listed in Table 1, it is estimated that the calibration procedure removes at least 90% of the error. Therefore, those bias errors are multiplied by 0.1 before being propagated into ρ.

In studying the propagation of uncertainties into ρ, it is helpful to recognize that the bias uncertainty in C_l and in C_g is not a new, independent uncertainty contribution, but is exactly the same as that already represented in C, so the procedure described in the previous paragraph is a convenient short cut to treating the bias uncertainty. The random uncertainty component in C_l and C_g is usually negligible compared to that in C, because the C_l and C_g values are usually obtained by averaging C values over some time interval. Therefore, for purposes of uncertainty propagation, it is acceptable and convenient to neglect the uncertainty in C_l and C_g and to reduce the effective magnitude of the bias uncertainty in C by the factor 0.1.

The derivatives of Equation (36) can be used in Equation (13) to give

$$(\sigma\rho)^2 = \left[\frac{\ln (C_g/C)}{\ln (C_g/C_l)}\right]^2 (\sigma\rho_l)^2 + \left[\frac{\ln (C/C_l)}{\ln (C_g/C_l)}\right]^2 (\sigma\rho_g)^2$$

$$+ \left[\frac{\rho_g - \rho_l}{\ln (C_g/C_l)}\right]^2 \left(\frac{\sigma C}{C}\right)^2 = \left[\frac{\rho - \rho_g}{\rho_l - \rho_g}\right]^2 (\sigma\rho_l)^2$$

$$+ \left[\frac{\rho_l - \rho}{\rho_l - \rho_g}\right]^2 (\sigma\rho_g)^2 + b^2 \left(\frac{\sigma C}{C}\right)^2 . \qquad (37)$$

The b in Equation (37) is the same as the calibration coefficient b in Equations (7) and (8). Equation (37) is applicable to the normal calibration procedure, and the values from Equations (32) and (33) should be used in Equation (37).

If the theoretical value of b is used instead of the measured C_g for calibration, the applicable equation for $\sigma\rho$ is

$$(\sigma\rho)^2 = (\sigma\rho_l)^2 + (\rho_l - \rho)^2 \left(\frac{\sigma b}{b}\right)^2 + b^2 \left(\frac{\sigma C}{C}\right)^2 . \qquad (38)$$

Values from Equations (33) and (35) should be used in Equation (38).

Equations (37) and (38) should account for the effects of all the uncertainty sources discussed so far, except that the uncertainty contribution associated with R was not included in the C uncertainty and must be added separately to the ρ uncertainty. These contributions to the ρ uncertainty are summarized in Table 4. The range for the random errors represents the worst case (high fluid density, maximum background radiation intensity) to the best case (low density, zero background) conditions. The two values for bias error correspond to the normal calibration procedure or the theoretical calibration procedure. The values for the $\sigma\ \rho_l$ and $\sigma\ \rho_g$ contributions are the worst case values; uncertainties may be considerably smaller for ρ values closer to ρ_l or ρ_g.

The random component of $\sigma\ \rho$ in Table 4 is for the minimum 12.5-ms data averaging time. If, as is frequently done, the data are averaged over a longer time T, then the random component of $\sigma\ \rho$ is reduced by the factor $\sqrt{12.5\ \text{ms}/T}$, approximately. This reduction factor is not exact, because the usually minor effect of the truncation error in P′ is not always reduced by averaging the data for a longer time, depending on the details of the averaging procedure. However, this uncertainty component is insignificant for T less than 12 seconds, which is a very long averaging time for normal experiment data, so the noise reduction factor given above is normally a good approximation.

This noise reduction factor is incorporated into Table 5, which summarizes the measurement uncertainties in terms of 2σ (95% confidence level) bands. Note that all the previously stated values represented the more natural and convenient 1σ levels.

4.18 Electronics Malfunction

Significant malfunctions in the data acquisition and recording electronics usually result in gross and obvious errors in the recorded data; in which case, the affected beam is declared failed and the data are not used. Those rare malfunctions that might result in plausible, but erroneous, data are exceedingly difficult to predict and analyze, and they are not treated here.

TABLE 4. CONTRIBUTIONS TO $\sigma\rho$ (Mg/m^3)

Source	Type	Magnitude of Uncertainty Component		
		Beam A	Beam B	Beam C
$\sigma C/C$	Bias	0.007	0.006	0.010
$\sigma C/C$	Random	0.091 to 0.137	0.076 to 0.114	0.147 to 0.247
$\sigma C/C$	Other	0.020	0.027	0.018
σR	Bias	0.004	0.006	0.003
$\sigma\rho_l$	Bias	<0.006	<0.006	<0.006
$\sigma\rho_g$ or σb	Bias	<0.001 or <0.05	<0.001 or 0.05	<0.001 or <0.05
Total bias		<0.010 or <0.051	<0.010 or <0.051	<0.012 or <0.051
Total random		0.091 to 0.137	0.076 to 0.114	0.147 to 0.247
Total other		0.020	0.027	0.018
Total $\sigma\rho$:				
Low density and normal calibration		<0.094	<0.082	<0.149
High density and normal calibration		<0.139	<0.118	<0.248
Low density and theoretical calibration		<0.106	<0.095	<0.157
High density and theoretical calibration		<0.148	<0.128	<0.253

TABLE 5. MEASUREMENT UNCERTAINTY SUMMARY

Conditions	Measurement Uncertainty, 2σ or 95% Confidence Level (Mg/m^3)		
	Beam A	Beam B	Beam C
Low density and normal calibration	$\sqrt{0.0020+0.00041/T}$	$\sqrt{0.0033+0.00029/T}$	$\sqrt{0.0019+0.00108/T}$
High density and normal calibration	$\sqrt{0.0020+0.00094/T}$	$\sqrt{0.0033+0.00065/T}$	$\sqrt{0.0019+0.00305/T}$
Low density and theoretical calibration	$\sqrt{0.012+0.00041/T}$	$\sqrt{0.013+0.00029/T}$	$\sqrt{0.012+0.00108/T}$
High density and theoretical calibration	$\sqrt{0.012+0.00094/T}$	$\sqrt{0.013+0.00065/T}$	$\sqrt{0.012+0.00305/T}$
Worst case: T = 0.0125[a], high density, and theoretical calibration	0.30	0.26	0.51
Best case: Very large T, low density, and normal calibration	0.05	0.06	0.05
Typical fast transient test: T = 0.05, high density, and normal calibration	0.14	0.13	0.25
Typical slow transient test: T = 1.0, high density, and theoretical calibration	0.11	0.12	0.12

a. T is the data averaging time in seconds.

5. CONCLUSIONS

The major uncertainty components in the LOFT radiation-hardened densitometers are the random noise associated with the radiation process randomness and the bias uncertainty associated with the theoretical calibration procedure (if the theoretical calibration is used). The random noise can be reduced by averaging data over longer time periods, if slower response is acceptable. Otherwise, the random noise cannot be significantly reduced without major densitometer design changes.

6. REFERENCES

1. D. L. Reeder, *LOFT System and Test Description (5.5-ft. Nuclear Core 1 LOCEs)*, NUREG/CR-0247, TREE-1208, July 1978.

2. G. D. Lassahn, *LOFT Experimental Measurements Uncertainties Analyses, Volume XVI, LOFT Three-Beam Gamma Densitometer System*, TREE-NUREG-1089, February 1978.

3. M. McCormick-Barger, *Experiment Data Report for LOFT Power Ascension Test L2-2*, NUREG/CR-0492, TREE-1322, February 1979.

4. P. G. Prassinos, B. M. Galusha, D. B. Engelman, *Experiment Data Report for LOFT Power Ascension Experiment L2-3*, NUREG/CR-0792, TREE-1326, July 1979.

5. P. G. Prassinos, B. M. Galusha, D. B. Jarrell, *Experiment Data Report for LOFT Nonnuclear Small Break Experiment L3-0*, NUREG/CR-0959, TREE-1390, August 1979.

EG&G Idaho, Inc.
P.O. Box 1625
Idaho Falls, Idaho 83415